AIAA JOURNAL
Vol. 45, No. 7, July 2007

Real-Time Prediction of Incipient Lean Blowout in Gas Turbine Combustors

Tongxun Yi* and Ephraim J. Gutmark†
University of Cincinnati, Cincinnati, Ohio 45220-0070

DOI: 10.2514/1.25847

The present paper addresses real-time prediction of incipient lean blowout in partially premixed, liquid-fueled gas turbine combustors. Near-lean-blowout combustion is characterized by the intensified, low-frequency combustion oscillations (typically, below 30 Hz). Two indices, namely, the normalized chemiluminescence root mean square and the normalized cumulative duration of lean blowout precursor events, are recommended for lean blowout prediction. Both indices are associated with the statistical characteristics of the flame structure, which changes from the normal distribution to the Rayleigh distribution at the approach of lean blowout. Both indices change little within a large range of equivalence ratios and start to shoot up only when lean blowout is approached. To use the two indices for lean blowout prediction, one needs to perform a detailed a priori lean blowout mapping undersimulated engine operating conditions. However, the mapping can be done without running the engines very close to lean blowout.

Nomenclature

F_s	=	sampling frequency, Hz
N	=	sample length
Q	=	air flow rate, g/s
$\bar{q}$	=	OH* chemiluminescence mean, V
q_i	=	ith sample of OH* chemiluminescence, V
q'_i	=	filtered OH* chemiluminescence with a bandpass filter, V
$\tilde{q}_i$	=	filtered OH* chemiluminescence with a high-pass filter, V
RMS_b	=	root mean square of q'_i, V
RMS_h	=	root mean square of $\tilde{q}_i$, V
T_0	=	preheat temperature, K
Θ	=	normalized cumulative duration of lean blowout precursor events
Φ	=	equivalence ratio
Φ_{lbo}	=	the lean blowout limit (the equivalence ratio at which lean blowout occurs)

I. Introduction

TO achieve the lowest possible NO_x, modern gas turbine engines are typically designed to operate in lean premixed or partially premixed mode [1]. Because of the low flame temperature and the lack of hot regions for flame stabilization, lean blowout (LBO) has become a major technical challenge for dry-low-emission gas turbines, especially when they are operating at low-power conditions [1]. LBO is a significant safety hazard for aeroengines and necessitates an expensive and time-consuming shutdown and restarting procedure for stationary engines. Accurate prediction and effective control of LBO help to enhance the flight safety, improve the operational economy, and reduce the overall emissions.

Accurate theoretical prediction of LBO is challenging, because many fundamental mechanisms in flame ignition, stabilization, and propagation remain unknown, despite extensive research in the past several decades. Phenomenological detection of LBO seems to be a viable approach. Lefebvre [2] pioneered the approach of correlation-function-based LBO prediction, which is very useful for combustor design, but may not be accurate enough for online LBO prediction. Barnum and Bell [3] and Lucenko et al. [4] proposed to detect LBO based on the decreasing rates of the combustor pressure and the compressor rotating speed, but the detecting speed is low. Snyder and Rosfjord [5] proposed to predict the LBO onset based on pressure fluctuations in the combustor; however, it is difficult to infer the procedures from [5]. Muruganandam et al. [6] studied LBO in a premixed, swirl-stabilized, methane-fueled combustor using OH* chemiluminescence. They identified the LBO precursors as short-duration, localized flame extinction and reignition events, and they found that these events increased in frequency and duration as LBO was approached. It is worthwhile to point out that intensified, low-frequency, near-LBO combustion oscillations have been widely reported in combustion literature, which may be associated with the intrinsic flame instabilities [7–9]. Yi and Gutmark [10] show that the flame's robustness to external disturbances becomes considerably weakened when LBO is approached. Near-LBO combustion may remain stable in the presence of small disturbances, but may undergo subcritical bifurcations to flame quenching when the external disturbances exceed certain thresholds. This is somewhat similar to the triggered instability in solid rocket engines [11]. It is found that both incomplete combustion and heat loss exacerbate the lean flame stability [10].

A natural approach to extend the LBO limit Φ_{lbo} is to increase the amount of pilot fuel [6]. However, excessive pilot fuel exacerbates CO and unburned hydrocarbons (UHC). One of the reviewers has some comments about this approach, which are copied here, verbatim, "the emissions penalty associated with increasing the pilot fuel flow rate is typically disproportionately higher than designing the combustor to run stably at higher overall equivalence ratios with lower amount of pilot fuel." Small-amplitude fuel modulations, based on the feedback control principles, might be employed to strengthen the flame's robustness to external disturbances, without sacrificing the overall emissions. Yi and Gutmark [10] numerically demonstrated the effectiveness of this control approach using a nonlinear well-stirred-reactor (WSR) model. However, further experimental verifications are required.

The present paper investigates the LBO phenomenology in a partially premixed, turpentine-fueled, multiswirl-stabilized, atmospheric gas turbine combustor. Several statistical approaches are used to quantify the low-frequency near-LBO combustion oscillations. Two indices, namely, the normalized chemiluminescence root mean square (RMS) and the normalized cumulative duration of LBO

Presented as Paper 959 at the 44th AIAA Aerospace Sciences Meeting and Exhibit, Reno, NV, 9–12 January 2006; received 13 June 2006; revision received 23 November 2006; accepted for publication 16 December 2006.

*Graduate Assistant, Department of Aerospace Engineering; yit@email.uc.edu. Student Member AIAA (Corresponding Author).

†Ohio Eminent Scholar, Professor, Department of Aerospace Engineering. Associate Fellow AIAA.

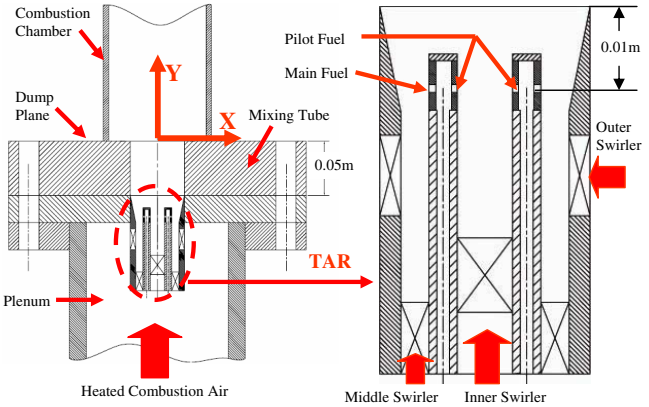

Fig. 1 Atmospheric combustion rig and TARS.

precursor events are recommended for LBO prediction in genetic gas turbine engines.

II. Experimental Setup

A. Combustion Rig

A combustion simulator should have similar flow patterns and thermochemistry to those of a generic gas turbine combustor. Several similarity criteria have been discussed by Penner in the 1950s [12]. Figure 1 shows the atmospheric combustion rig featured with the triple annular research swirler (TARS). The combustion chamber is a 0.30-m-long quartz tube with an internal diameter of 0.15 m. The TARS has three air swirlers, with the inner swirl angle at 30 deg (clockwise), the middle one at 45 deg (clockwise), and the outer one at 55 deg (counterclockwise). A 0.05-m-long mixing tube is installed at the TARS exit to improve fuel/air mixing and reduce the overall emissions. The corrected CO (15% O_2, dry) is typically below 20 ppm for $\Phi = 0.5$, and the corrected NO_x is typically below 10 ppm for $\Phi < 0.55$. The TARS has two fuel lines, namely, the main fuel and the pilot fuel. The 1-decene is injected into the swirling air at 0.06 m upstream of the burner. The main fuel is injected between the outer and the middle air swirlers, and the pilot fuel is injected between the inner and the middle air swirlers. The main and the pilot fuel lines have separate manifolds. Two turbine flowmeters (HIT-2A from the Hoffer Flow Control, Inc.) are used for fuel flow rate measurement, with a measurement uncertainty of 0.04 g/s. The air-side pressure drop across the TARS is within 3–7% of the plenum pressure, which mainly depends on the air flow rate and the preheat temperature. Q is measured with an EPI thermal wire digital flowmeter, with a measurement uncertainty of 0.05 g/s. In most tests, Q is 55.6 g/s. The uncertainty of equivalence ratios is 0.01.

B. Fuel System

1-decene is pressurized at 1034 kPa with nitrogen and is delivered to the TARS in two streams, with one stream as the main fuel and the other as the pilot fuel. A Goodrich fuel valve is used to control the total fuel flow rate with a LQG pulse-width-modulation controller [13]. The fuel split ratio (FSR) is adjusted with two throttle valves installed in the main and the pilot fuel lines, respectively. The FSR is defined as the ratio of the main fuel flow rate to the total fuel flow rate.

C. Instrumentation

A DSpace system is used to control the Goodrich fuel valve. Data acquisition is done using a NI DAQ board (PCI-MIO-16XE-10). The sampling frequency is 5000 Hz. A B&K microphone with a sensitivity of 10 mV/Pa is installed at 0.23 m above the dump plane and 0.41 m away from its center. Type-B thermocouples and an F150 precision thermometer from ASL are used for temperature measurement. The radiative heat loss is compensated according to the procedures described in [14]. Temperature correction increases with Φ and can be up to 150 K for $\Phi > 0.6$. OH* chemiluminescence, which is converted to a voltage via a photomultiplier tube that is used for line-of-sight heat release rate measurement. A high-resolution super blue ICCD camera from Roper Scientific is used for global flame visualization. Exhaust species are sampled at the center of the combustor exit with a ceramic probe. CO, CO_2, and O_2 are measured with an infrared gas analyzer, and NO_x is measured with a chemiluminescence gas analyzer from California Analytical Instruments. The measurement uncertainty is 1 ppm for NO_x and 3 ppm for CO.

III. Near-LBO Phenomenology

LBO is approached by stepwise, small reductions in the total fuel flow rate, whereas the FSR, Q, and T_0 are kept constant. A larger incremental reduction in Φ of about 0.03 is used when combustion is well above LBO, whereas a smaller incremental reduction in Φ of about 0.01 is used when combustion is close to LBO. After each decrement in Φ, it usually takes about 20 s for the temperature measured at the combustor exit to reach a new equilibrium state. This long transient is mainly associated with the heat loss to the rig and the surroundings. The data presented and analyzed in the present paper are obtained after the transient period.

Both pressure and chemiluminescence can be used to probe the near-LBO combustion dynamics. Please note that in the present paper, combustion dynamics simply refers to the temporal evolution of OH* chemiluminescence or pressure, instead of the combustion instability. The frequency range of near-LBO combustion oscillations is typically below 30 Hz, much below the acoustic resonant frequencies, and so pressure is not as sensitive as chemiluminescence for LBO detection. The present paper focuses on optical sensing.

The near-LBO flame structure is very sensitive to the working conditions (especially, the FSR) and the combustor geometry. Limited by space, the detailed flame structures are not enumerated in the present paper. A recent study characterizes the near-LBO combustion dynamics as low-dimension chaotic behavior [15]. Chaotic systems are sensitive to tiny variations in the initial and the boundary conditions [16], which may explain the rich variety of near-LBO flame structures. In our experiments, intensified, low-frequency, near-LBO combustion oscillations are found to correlate with the large-scale flame extinction and reignition events within the swirling shear layer. Figure 2 shows the time traces of OH* chemiluminescence and pressure at $\Phi = 0.45$ and $\Phi = 0.42$, respectively. Here, FSR = 55%, $T_0 = 573$ K, $Q = 55.6$ g/s, and $\Phi_{lbo} = 0.42$. OH* chemiluminescence is measured at 0.10 m above the dump plane, with a view angle of about 30 deg. At $\Phi = 0.42$, chemiluminescence oscillations are quite random and noncoherent, which is in sharp contrast to combustion instability. This is mainly because combustion instability involves the positive feedback

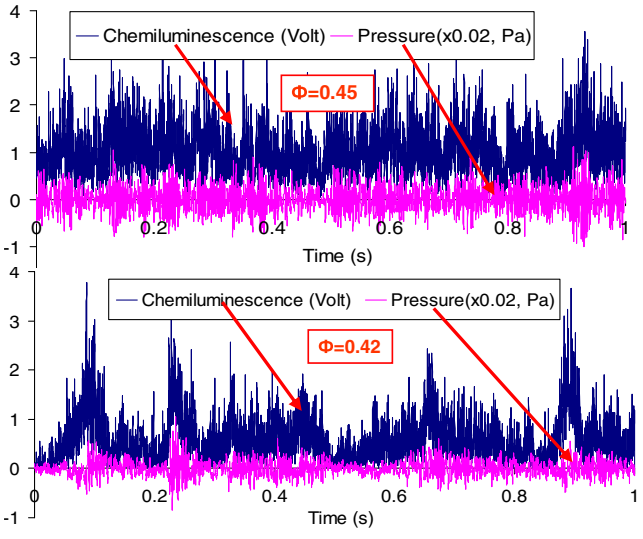

Fig. 2 Typical time traces of pressure and OH* chemiluminescence.

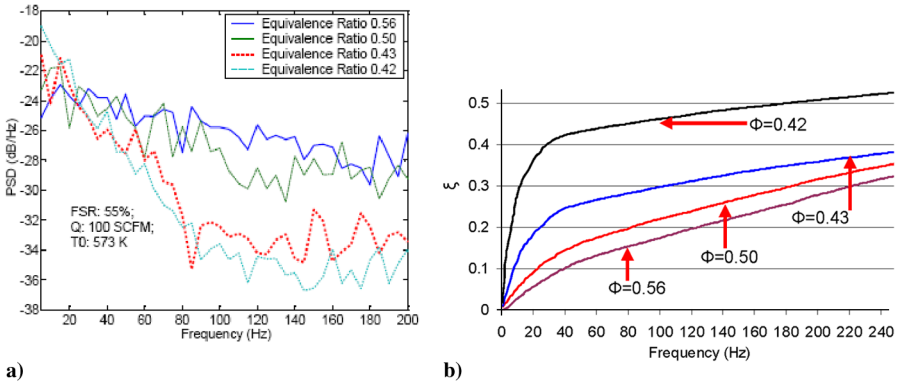

a) b)

Fig. 3 Spectral characteristics of chemiluminescence at the approach of LBO: a) power density spectrum and b) percentage of the cumulative energy.

between pressure and the heat release rate, whereas the near-LBO combustion oscillations usually do not.

IV. Statistical Analyses of Near-LBO Phenomenology

A. Spectral Analysis

Figure 3a compares the power density spectrum of OH* chemiluminescence at different equivalence ratios. Here, FSR = 55%, $T_0 = 573$ K, $Q = 55.6$ g/s, $\Phi_{\text{lbo}} = 0.42$, and $N = 50,000$. The power density spectrum drops much faster with the frequency at $\Phi = 0.43$ and 0.42 than that at $\Phi = 0.50$ and 0.56. The trend of decreasing amplitude with the frequency is a typical feature of chaotic systems. A cumulative distribution function $\xi(i)$ is defined to quantify the energy distribution with the frequency:

$$\xi(i) = \sum_{k=1}^{i} H_k^2 \Big/ \sum_{k=1}^{2500} H_k^2 \qquad (k = 1, 2, \ldots, 2500) \tag{1}$$

H_k refers to the amplitude of OH* chemiluminescence at the kth pin in fast Fourier transform (FFT) analysis. Figure 3b shows that the low-frequency components of OH* chemiluminescence have a much higher energy percentage at $\Phi = 0.43$ and 0.42 than that at $\Phi = 0.50$ and 0.56. The fact that the low-frequency components dominate the near-LBO combustion dynamics may suggest the possibility of low-order modeling and control of LBO.

B. Autocorrelation Function

The autocorrelation function is commonly used to determine if any determinism exists in the experimental data. If determinism does exist, a linear or nonlinear time series model may be developed [17]. The autocorrelation coefficient (AC) at the kth time lag is defined as

$$r_k = \sum_{i=1}^{N-k} (q_i - \bar{q})(q_{i+k} - \bar{q}) \Big/ \sum_{i=1}^{N} (q_i - \bar{q})^2 \qquad \bar{q} = \sum_{i=1}^{N} q_i \Big/ N \tag{2}$$

If a process is purely random, the AC will be zero anywhere except at the time lag of zero. A chaotic system is deterministic; however, a high-dimension chaos may also exhibit randomlike behavior [18]. Thus, a small AC does not necessarily imply that the process is truly random. Figure 4 compares the AC at different equivalence ratios. Here, FSR = 55%, $T_0 = 573$ K, $Q = 55.6$ g/s, $\Phi_{\text{lbo}} = 0.42$, and $N = 10,000$. At the same time lag, the AC consistently increases at the approach of LBO, suggesting that combustion oscillations become more deterministic and can be more accurately predicted by low-order models. Note that the output voltage of the photomultiplier tube may be contaminated by power-line electrical noises. However, these noises occur within certain narrow frequency ranges and can be easily filtered out with bandstop filters.

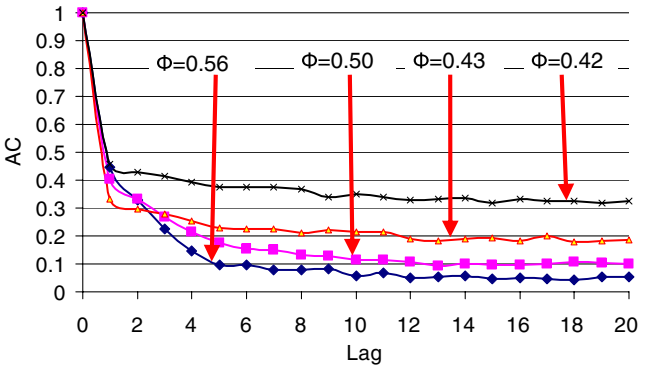

Fig. 4 Autocorrelation coefficients of chemiluminescence.

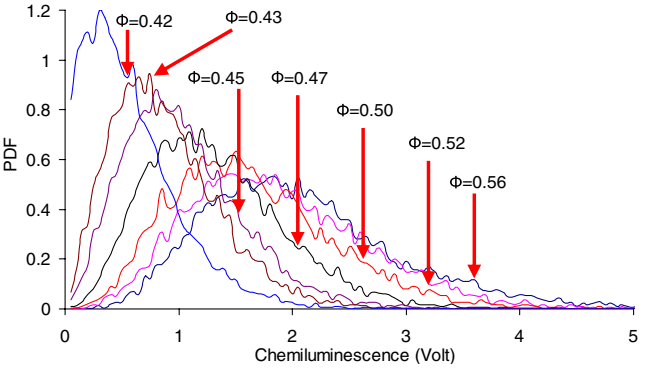

Fig. 5 PDF of OH* chemiluminescence.

C. Probability Density Function

Figure 5 compares the probability density function (PDF) of OH* chemiluminescence at different equivalence ratios. Here, FSR = 55%, $T_0 = 573$ K, $Q = 55.6$ g/s, $\Phi_{\text{lbo}} = 0.42$, and $N = 10,000$. The PDF is based on the histogram for which the column width is 0.05 V. Because of the decreasing chemiluminescence mean, the peak of the PDF shifts to a lower value when LBO is approached. The PDF is more symmetric at a higher Φ than at a lower Φ. Figure 6 compares the PDF of OH* chemiluminescence with the normal and the Rayleigh distributions at $\Phi = 0.43$ and 0.56, respectively. Interested readers may refer to [19] for the definitions of the Rayleigh and the normal distributions. The normal distribution is uniquely determined by the mean and the standard deviation of a random process, whereas the Rayleigh distribution is only associated with the standard deviation. Figure 6a shows that for near-LBO combustion (say, at $\Phi = 0.43$), the PDF of OH* chemiluminescence can be better described by the Rayleigh distribution than by the normal distribution. However, Fig. 6b suggests that for combustion above LBO (say, at $\Phi = 0.56$), the PDF of OH* chemiluminescence can be better described by the normal distribution than by the

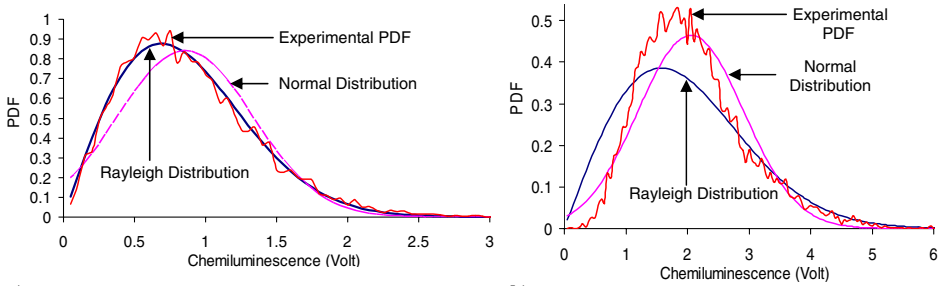

Fig. 6 Experimental PDF vs the normal and the Rayleigh distribution: a) $\Phi = 0.43$ and b) $\Phi = 0.56$.

Rayleigh distribution. As will be discussed later in the present paper, the variations in the statistical properties of OH* chemiluminescence can be used for LBO prediction.

D. Quantifying the Low-Frequency Combustion Oscillations

The intensity of near-LBO combustion oscillations can be quantified by the RMS of OH* chemiluminescence:

$$\text{RMS} = \sqrt{\sum_{i=1}^{N}(q_i - \bar{q})^2 \Big/ N} \tag{3}$$

However, Eq. (3) is not suitable for real-time computation, because the chemiluminescence mean $\bar{q}$ is not known until at the end of the Nth sample. To improve the real-time performance, $q_i - \bar{q}$ can be approximated by $\tilde{q}_i$, which is the filtered chemiluminescence with a high-pass filter (say, with the cutoff frequency of 2 Hz). Denote the RMS of $\tilde{q}_i$ as RMS_h:

$$\text{RMS}_h = \sqrt{\sum_{i=1}^{N}(\tilde{q}_i)^2 \Big/ N} \tag{4}$$

Because the low-frequency, near-LBO combustion oscillations typically occur within the low-frequency range, a more reasonable index is the RMS of q_i', which is the filtered chemiluminescence with a bandpass filter (say, with the bandwidth of 2–100 Hz). Denote the RMS of q_i' as RMS_b:

$$\text{RMS}_b = \sqrt{\sum_{i=1}^{N}(q_i')^2 \Big/ N} \tag{5}$$

Table 1 compares RMS, RMS_h, and RMS_b at different equivalence ratios. Here, FSR = 55%, $T_0 = 573$ K, $Q = 55.6$ g/s, $\Phi_{\text{lbo}} = 0.42$, and $N = 10,000$. All these indices consistently decrease when LBO is approached, whereas $\text{RMS}_b/\text{RMS}_h$ consistently increases. Thus, one can conclude that what is really increasing at the approach of LBO is the energy percentage, rather than the absolute energy of the low-frequency components. The difference between RMS and RMS_h is less than 3.5%, and so RMS_h well approximates RMS. Table 1 also shows the normalized chemiluminescence RMS, that is, NRMS:

$$\text{NRMS} = \text{RMS}_b/\bar{q} \tag{6}$$

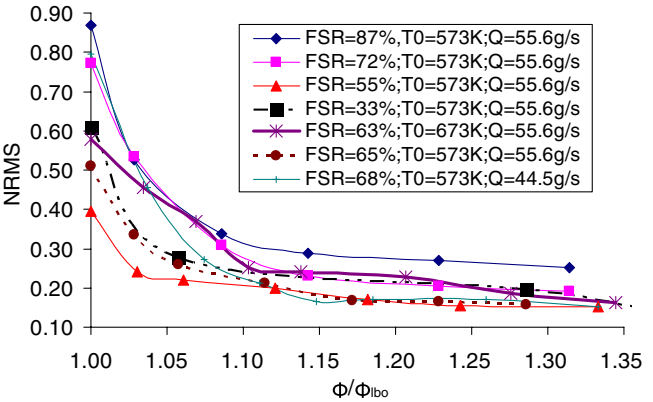

Fig. 7 Different working conditions of NRMS.

where NRMS can be interpreted as the ratio of the standard deviation to the chemiluminescence mean.

Figure 7 compares NRMS at different working conditions; NRMS increases slowly with decreasing equivalence ratios until $\phi/\phi_{\text{lbo}} < 1.15$. This trend has been confirmed by other researchers [20,21], who observed that the heat release RMS was roughly proportional to the mean heat release rate. To compute NRMS, one needs to specify a time window or a sample length N. Because of the chaotic and seemingly irregular feature of near-LBO combustion dynamics, a larger N is preferred. However, a larger N will inevitably slow down the detecting speed. Figure 8 shows that a sample length of 10,000 is capable of achieving a reasonable balance between the accuracy and the detecting speed.

Muruganandam et al. [6] used a threshold-based approach to count the LBO precursor events, and the occurrence rate is taken as a measure of the LBO proximity. According to their approach, a LBO precursor event occurs "whenever the OH signal drops below (somewhat arbitrarily chosen) value equal to one quarter of the mean signal value. This choice is based on the premise that the precursor signature is initiated by a local extinction event that temporarily lowers the chemiluminescence." [6]. In the present paper, instead of counting the LBO precursor rate, a normalized cumulative duration of LBO precursor events Θ is computed:

$$\Theta = N_t/N \tag{7}$$

N_t denotes the number of samples for which the value is below a

Table 1 Comparisons between RMS, RMS_h, RMS_b, and NRMS.

		RMS	RMS_h	Error, %	RMS_b	$\text{RMS}_b/\text{RMS}_h$, %	$\bar{q}$	NRMS
ϕ	0.56	0.8592	0.8880	3.3760	0.3109	35.02	2.0541	0.2078
	0.52	0.7776	0.8014	2.9563	0.2869	35.81	1.8476	0.2135
	0.50	0.7143	0.7296	2.2409	0.2778	38.10	1.6216	0.2265
	0.47	0.6061	0.6232	2.8053	0.2567	41.24	1.2957	0.2531
	0.45	0.5221	0.5275	1.1494	0.2229	42.27	1.0112	0.2772
	0.43	0.4740	0.4756	0.4219	0.2074	43.52	0.8563	0.2909
	0.42	0.4167	0.4079	2.1583	0.1932	47.36	0.5557	0.4514

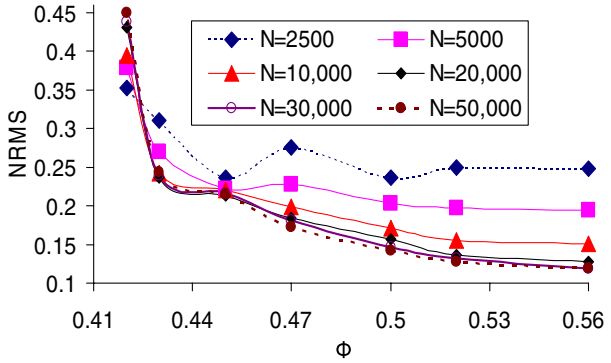

Fig. 8 Effects of N on NRMS.

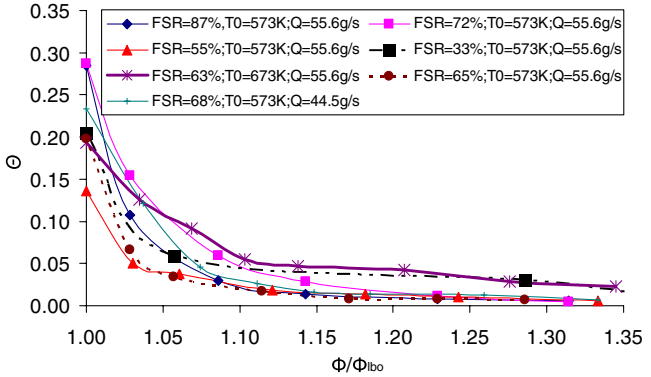

Fig. 9 Normalized cumulative duration of LBO precursor events at different working conditions.

certain threshold (say, $0.20\bar{q}$). The LBO precursor events occur rather randomly both in the frequency and duration; however, Θ takes both effects into account. Figure 9 shows Θ at different working conditions. Similarly to NRMS, shown in Fig. 7, Θ increases very slowly until $\phi/\phi_{\text{lbo}} < 1.15$. Note that NRMS and Θ are mathematically interdependent. Figure 6 shows that for combustion well above LBO, the PDF of OH* chemiluminescence can be approximated by the normal distribution. Figure 7 shows that at a fixed FSR, the ratio of the standard deviation to the chemiluminescence mean (i.e., the NRMS) is roughly a constant. Thus, the PDF of the normalized chemiluminescence (i.e., $q_i/\bar{q}$) is almost invariant at a fixed FSR for $\phi/\phi_{\text{lbo}} > 1.15$. One can also see that Θ is simply the cumulative probability for $q_i/\bar{q} < 0.20$. This explains why Θ remains almost constant at the same FSR until $\phi/\phi_{\text{lbo}} < 1.15$. However, at this moment, it is unclear whether the qualitative change in the flame structure always occurs at $\phi/\phi_{\text{lbo}} \approx 1.15$ or not.

The results shown in Figs. 7 and 9 are based on the OH* chemiluminescence observed within two s. Because of the chaotic feature of combustion oscillations, both NRMS and Θ vary with time, even at the same working conditions. In addition, the variations in the inlet turbulence and fuel compositions also introduce combustion oscillations. However, both NRMS and Θ are reproducible. Table 2 shows NRMS and Θ for the LBO experiments, which were repeated three times within six months. Here, FSR = 66%, $T_0 = 573$ K, $Q = 55.6$ g/s, $\Phi_{\text{lbo}} = 0.45$, and $N = 10,000$. For each experiment, OH* chemiluminescence is sampled for more than 1 min, and both NRMS and Θ are computed for every two s. In Table 2, $\overline{\text{NRMS}}$ and $\bar{\Theta}$ denote the mean of NRMS and Θ, respectively, and $\sigma(.)$ denotes the standard deviation. Within a period of six months, $\sigma(\text{NRMS})/\overline{\text{NRMS}}$ is less than 5% and $\sigma(\Theta)/\bar{\Theta}$ is less than 15% for $\phi/\phi_{\text{lbo}} > 1.15$. Larger variations in NRMS and Θ occur for $\phi/\phi_{\text{lbo}} < 1.15$, however, they are still below 20%.

V. LBO Prediction

The present paper recommends that either NRMS or Θ be used for real-time prediction of incipient LBO in generic gas turbine engines. These two indices are mathematically dependent, as explained in the previous section. Both NRMS and Θ require few computations within each sample interval, and so the real-time requirement is satisfied. The lean blowout limit is a function of FSR, T_0, and, probably, Q. Even at fixed working conditions, Φ_{lbo} cannot be uniquely determined, because of the chaotic feature of near-LBO combustion dynamics and the external disturbances. The present paper suggests that a LBO warning be initiated when the following condition is satisfied:

$$\frac{\text{NRMS}(\text{FSR}, T_0, Q, \phi/\phi_{\text{lbo}})}{\text{NRMS}(\text{FSR}, T_0, Q, \phi/\phi_{\text{lbo}} > 1.15)} > \alpha \quad \text{or} \quad \frac{\Theta(\text{FSR}, T_0, Q, \phi/\phi_{\text{lbo}})}{\Theta(\text{FSR}, T_0, Q, \phi/\phi_{\text{lbo}} > 1.15)} > \alpha \tag{8}$$

The preceding prediction mechanism does not require the knowledge of NRMS and Θ at or near Φ_{lbo}. However, one does need to have good estimates for NRMS and Θ at the present FSR, T_0, and Q for combustion above LBO. One of the reviewers pointed out that to obtain such information, a detailed a priori mapping of NRMS and Θ undersimulated gas turbine operating conditions is necessary. However, the mapping task is not formidable. On one hand, neither NRMS nor Θ is very sensitive to equivalence ratio variations until $\phi/\phi_{\text{lbo}} < 1.15$, and so the mapping can be done without running the engines very close to LBO, thus the expensive and time-consuming shutdown and restarting procedures can be avoided; on the other hand, the mapping can be combined with routine combustion tests. For example, a stationary gas turbine manufactured by GE will be comprehensively tested at the factory and will be tested again at the customer's site [22]. The value of α in Eq. (8) is suggested to be 1.75. Although stable combustion could still be maintained for $\alpha > 1.75$, the flame's robustness to external disturbances is considerably weakened [10]. Thus, α should not be too large. Here, we examine the effects of NRMS and Θ variations on LBO prediction. As shown in Table 2, both NRMS and Θ exhibit oscillations at fixed working conditions, but the relative oscillating magnitude is below 20%. By setting $\alpha = 1.75$, the oscillations in NRMS and Θ will not obscure LBO prediction. As soon as LBO warning is initiated, active control systems should be immediately put into operation to strengthen the lean combustion stability. This can be done either by increasing the

Table 2 Reproducibility of NRMS and Θ.

		NRMS			Θ		
		$\overline{\text{NRMS}}$	σ(NRMS)	$\sigma(\text{NRMS})/\overline{\text{NRMS}}$	$\bar{\Theta}$	$\sigma(\Theta)$	$\sigma(\Theta)/\bar{\Theta}$
ϕ/ϕ_{lbo}	1.29	0.1742	0.0060	3.44%	0.0059	0.0008	13.60%
	1.23	0.1771	0.0084	4.74%	0.0067	0.0007	11.04%
	1.17	0.1963	0.0084	4.28%	0.0093	0.0013	14.00%
	1.11	0.2340	0.0108	4.62%	0.0154	0.0018	11.49%
	1.06	0.3012	0.0177	5.88%	0.0355	0.0048	13.66%
	1.03	0.3682	0.0266	7.22%	0.0615	0.0111	18.03%
	1.00	0.5100	0.0890	17.50%	0.2178	0.0255	11.69%

pilot fuel [6] or, possibly, by using small-amplitude fuel modulations [10].

Two issues should be addressed before NRMS and Θ can be used for LBO detection in generic gas turbine engines. First, the operating conditions of an engine, such as the reacting flow pattern and spatial fuel distribution, may gradually change, possibly caused by combustor aging. Inevitably, one has to regularly update the mapping of NRMS and Θ. As mentioned before, this can be done without shutting down and restarting the engines, which saves time and cost and also favors the engines' longevity. Second, a generic gas turbine engine is featured with multiple nozzles or burners, and is typically operating above the atmospheric pressure. In gas turbine engines, usually several nozzles share the same pilot and main fuel lines. However, the fuel/air distribution for each of these nozzles may not be the same, possibly due to the minute differences in manufacturing, burner aging, and carbon contamination of the fuel injectors. Obviously, for accurate LBO prediction, the LBO mapping should be done for each nozzle or burner. In addition, chemiluminescence interferences from neighboring nozzles may complicate LBO detection. However, LBO is mostly associated with the radical pool established nearby the forward stagnation point of the vortex breakdown at the exit of each nozzle or burner, for which the flame interactions among neighboring nozzles are weak. By integrating the optical fibers with the fuel injectors or air swirlers and using small view angles, chemiluminescence interferences from neighboring nozzles may be effectively reduced or avoided. At high pressure, the chemical reaction rate increases; however, the laminar burning velocity is reduced [23], which may affect flame stabilization and propagation. Currently, the authors have no data for combustion above the atmospheric pressure and for multinozzle configurations. These two issues will be addressed in our future research.

VI. Conclusions

The present paper analyzes the lean blowout phenomenology in a partially premixed, turpentine-fueled, multiswirl-stabilized, atmospheric gas turbine combustor. It is found that near-LBO combustion dynamics is dominated by the intensified, low-frequency combustion oscillations (typically, below 30 Hz). The autocorrelation coefficient consistently increases at the approach of LBO, suggesting that near-LBO combustion becomes more deterministic. The probability density function of near-LBO OH^* chemiluminescence can be better described by the Rayleigh distribution than by the normal distribution. Two indices, namely, the normalized chemiluminescence RMS and the normalized cumulative duration of LBO precursor events, are recommended for LBO prediction in generic gas turbine engines. These two indices are statistically related and are repeatable at the same working conditions. Both indices change little within a large range of fuel/air equivalence ratios and start to shoot up only at the approach of LBO. To use either of the indices for LBO prediction, one needs to perform a detailed a priori mapping of the actual LBO undersimulated gas turbine operating conditions. However, the mapping can be done without running the engines very close to LBO, thus the expensive and time-consuming shutdown/restarting procedures are avoided. To reduce or avoid chemiluminescence interferences from neighboring nozzles/burners, the optical fibers should have small view angles and be integrated with the air swirlers or fuel injectors.

Acknowledgments

The authors would like to thank Nick Overman for assisting in the experiments. T. Yi is indebted to one of the anonymous reviewers for very instructive comments, such as the LBO thresholds determination, variations, repeatability, interdependence, and their susceptibility to chemiluminescence interferences from neighboring nozzles. T. Yi also wants to thank another anonymous reviewer for the insightful comments about LBO control.

References

[1] Lefebvre, A. H., "The Role of Fuel Preparation in Low-Emission Combustion," *Journal of Engineering for Gas Turbines and Power*, Vol. 117, 1995, pp. 617–665.

[2] Lefebvre, A. H., *Gas Turbine Combustion*, Taylor and Francis, Philadelphia, 1999, p. 187.

[3] Barnum, B. M., and Bell, R. C., "Flame Failure Detection Method," US Patent 5235802, filed 17 August 1993.

[4] Lucenko, M., Vanderleest, R. E., and Kenneth, J., "Method and Apparatus for Detecting Burner Blowout," U.S. Patent No. 5581995, filed 10 Dec. 1996.

[5] Snyder, T. S., and Rosfjord, T. J., "Active Gas Turbine Combustion Control to Minimize Nitrous Oxide Emissions," U.S. Patent No. 5706643, filed 13 Jan. 1998.

[6] Muruganandam, T. M., Nair, S., Scarborough, D., Neumeier, Y., Jagoda, J., Lieuwen, T., Seitzman, J., and Zinn, B., "Active Control of Lean Blowout for Turbine Engine Combustors," *Journal of Propulsion and Power*, Vol. 21, No. 5, 2005, pp. 807–814.

[7] Joulin, G., and Sinvashinsky, G. I., "Instability-Induced Quenching of Plane Non-Adiabatic Flames," *Combustion Science and Technology*, Vol. 55, 1987, pp. 83–88.

[8] Ju., Y., Law, C. K., Maruka, K., and Niloka, K., "Flame Bifurcations and Flammable Regions of Radiative Counterflow Premixed Flames with General Lewis Numbers," *28th International Combustion Symposium*, Vol. 28, Combustion Inst., Pittsburgh, PA, 2000, pp. 1891–1900.

[9] Kukuck, S., and Matalon, M., "The Onset of Oscillations in Diffusion Flames," *Combustion Theory and Modeling*, Vol. 5, 2001, pp. 217–240.

[10] Yi, T., and Gutmark, E. J., "Effects of Chemical Kinetics and Heat Loss on Near-LBO Combustion Dynamics—Stability Analysis," AIAA Paper 2007-0388, Jan. 2007.

[11] Yang, V., Kim, S. I., and Culick, F. E. C., "Triggering of Longitudinal Pressure Oscillations in Combustion Chambers, 1: Nonlinear Gasdynamics," *Combustion Science and Technology*, Vol. 72, 1990, pp. 183–214.

[12] Penner, S. S., *Combustion Researches and Reviews*, Butterworths, London, 1955.

[13] Yi, T., and Gutmark, E. J., "Mean Flow Regulation of a High Frequency Fuel Actuator Based on Pulse Width Modulation and System Identification," *Proceedings of the 2005 American Control Conference*, American Automatic Control Council, Evanston, IL, and Inst. of Electrical and Electronics Engineers, Piscataway, NJ, 2005, pp. 1132–1137.

[14] Shaddix, C. R., "Correcting Thermocouple Measurements for Radiation Loss: a Critical Review," *Proceedings of the 33rd National Heat Transfer Conference* [CD-ROM], American Society of Mechanical Engineers, New York, 1999; also National Heat Transfer Conference Paper NHTC99-282.

[15] Yi, T., and Gutmark, E. J., "Characterization of Near-Blowout Combustion Oscillations in a Lean, Partially Premixed Gas Turbine Combustor," AIAA Paper 2006-4738, July 2006.

[16] Shinbrot, T., Ditto, W., Grebogi, C., Ott, E., Spano, M., and Yorke, J. A., "Using the Sensitive Dependence (the "Butterfly Effects") to Direct Trajectories in an Experimental Chaotic System," *Physical Review Letters*, Vol. 68, No. 19, 1992, pp. 2863–2866.

[17] Box, G. E. P., Jenkins, G. M., and Reinsel, G. C., *Time Series Analysis: Forecasting and Control*, Prentice–Hall, Englewood Cliffs, NJ,1994.

[18] Keanini, R., Yu, K., and Daily, J., "Evidence of a Strange Attractor in Ramjet Combustion," AIAA Paper 89-0624, Jan. 1989.

[19] Papoulis, A., *Probability, Random Variables, and Stochastic Processes*, McGraw–Hill, New York, 1984, pp. 100–101, 104–148.

[20] Lawn, C. J., "Distribution of Instantaneous Heat Release by the Cross-Correlation of Chemiluminescent Emission," *Combustion and Flame*, Vol. 123, Nos. 1–2, 2000, pp. 227–240.

[21] Langhorne, P. J., Bloxsidge, G. J., and Dowling, A. P., "Reheat Buzz: an Acoustically Coupled Combustion Instability," Parts 1 and 2, *Journal of Fluid Mechanics*, Vol. 193, 1988, pp. 417–473.

[22] Vandervort, C. L., "9 ppm NO_x/CO Combustion System for "F" Class Industrial Gas Turbines," ASME Turbo Expo 2000, Munich, Germany, American Society of Mechanical Engineers, Paper 2000-GT-0086, 2000.

[23] Turns, S. R., *An Introduction to Combustion: Concepts and Applications*, McGraw–Hill, Boston, 2000, p. 277.

J. Gore
Associate Editor